文章编号: 1001-9014(2019)03-0320-06 DOI: 10.11972/j.issn.1001-9014.2019.03.011

Enhanced optical transmission based on the electric field enhancement effect in a compact metal-dielectric double-layered films

ZHONG Min*

(Hezhou University, Hezhou 542899, China)

Abstract: Transmission enhancement is simulated verification based on a non-hollowing double layer of metamaterial filter. The proposed structure contains a continuous metallic film covering on a continuous dielectric layer. The simulated transmission is enhanced obviously comparing the single metal layer structure. Effects of the dielectric layer thickness and the incident angle on the transmission enhancement are simulated verification. It is found that the maximized transmittance enhancement is achieved when the thickness h1 is 20nm. Moreover, the proposed compact metal-dielectric double-layered films shows a stability of transmittance enhancement when the incident angle reaches to 45°, which can be applied in many potential fields due to its non-hollowing design strategy.

Key words: metamaterials, transmission, absorption
PACS: 41.20.Jb, 78.20.Cj, 73.20.Mf, 42.25.Bs

基于双层超材料中的电场增强效应增强光学透射

钟 敏*

(贺州学院,广西 贺州 542899)

摘要: 传输增强是基于非空心双层超材料滤波器的模拟验证. 所提出的结构包含覆盖在连续介电层上的连续金属膜. 与单金属层结构相比,模拟传输明显增强. 模拟验证了介电层厚度和入射角对传输增强的影响. 发现当厚度 h_1 为 20 nm 时,实现了最大化的透射率增强. 此外,所提出的紧凑金属-电介质双层薄膜在入射角达到45°时显示出透射率增强的稳定性,由于其非空心化设计策略,可以应用于许多潜在的领域.

关 键 词: 超材料; 传输; 吸收

中图分类号: O43 **文献标识码:** *A*

Introduction

Metamaterials have many unique properties, such as negative permeability, refractive index, and permittivity [1-2], etc. Metamaterials are used in multiple fields, including sub-diffraction imaging, optical black hole, and so on [3-7]. Among these applications, metamaterial filter is a research hotspot. Researchers have proposed a series of ways to enhance the transmittance of metamaterial filters [8-11]. *Krishnan A* experimental confirm the optical transmission enhanced due to the interaction between the incident light and surface plasmon modes [12]. *Lanju L* design and simulate a wideband band-pass terahertz filter based on stacking metal and material layers alternately [13]. *Lei W* adopts a simplified design strategy that designing and experimental preparing a low-pass filter in the terahertz regime with a single metal layer covering on a single chip [14]. In addition to optimizing the design strategy, another way to improve the transmission properties of metamaterial filters is to obtain impedance matching [15]. These reported results indicate that adopting structured design strategies to enhance transmission is a popular research method currently. However, this method always results in a complex targeted structure and an increase in requirements of the production equipment, which is not conducive to large-scale production as well as to reduce costs. On the other hand, the unstructured

Received date: 2018-09-08, **revised date:** 2018-12-19 **收稿日期:** 2018-09-08, **修回日期:** 2018-12-19
Foundation items: Supported by Doctor's scientific research foundation (HZUBS201503), Young and Middle Teachers' Basic Ability Improvement Project of Guangxi (KY2016YB453), Mathematical support autonomous discipline project of Hezhou University (2016HZXYSX01), and Innovation and entrepreneurship students project of Hezhou University (201611838018)
Biography: Zhong Min (1982-), male, Guangxi, research area involves: Engaged in the design and preparation of metamaterials, metasurfaces, graphene, etc.
* **Corresponding author:** E-mail: zhongmin2012hy@163.com

design strategy is a novel but unconcerned research method. This unstructured design strategy is to stack thin different materials films together to form a multilayer film structure. This structural design strategy has the following advantages: (a) the complicated production equipment is not required, (b) mass production, and (c) cost reduction. Therefore, unstructured multilayer film structure is worth studying.

In this paper, a material unstructured filter is designed and simulated. The proposed compact metal-dielectric double-layered films contain two materials: a metal layer covers on a nonmetallic layer. It is found that the transmission and absorption can be enhanced simultaneously, comparing to single metal layer structure. This indicates that the proposed compact metal-dielectric double-layered films show good high transmittance and conductivity simultaneously. This strategy only needs to cover a thickness appropriating layer of a dielectric layer on the metal layer that the transmittance enhanced effect is achieved. Therefore, the proposed compact metal-dielectric double-layered films can be applied in many fields, such as solar cells, liquid crystal display, light-emitting diodes, and so on.

1　Structural design and optimization

1.1　Structural design and theoretical model

The proposed compact metal-dielectric double-layered films are shown in Fig. 1(a). A silver layer covers on a glass substrate, and a $CaCO_3$ layer covers on the silver layer. Simulation is performed by the software Ansoft's HFSS 12.0. The proposed compact metal-dielectric double-layered films structure is a continuous structure in the xox plane, as shown in Fig. 1(a). A number of similar multilayer film structures have been reported [16-21]. The silver layer thickness is "h_2", the dielectric layer thickness is "h_1", and the glass substrate thickness is "h_3". In simulation, the lattice constant of the compact metal-dielectric double-layered films is "P". Moreover, the thickness h1 is an adjustable structural parameter in simulation. Four ideal boundaries are applied in the unit cell of the proposed compact metal-dielectric double-layered films [22]. These ideal boundaries ensure no electromagnetic wave energy between unit cells. In simulation, electromagnetic waves are incident perpendicularly to the surface of the structure. Specific structural parameters are given in Table 1. The silver layer is following the *Drude model* [23]. The simulated transmission is achieved as:

$$T(\lambda) = 1 - R(\lambda) - A(\lambda) \quad , \quad (1)$$

Here, $A(\lambda)$ is the simulated absorption rate, while $R(\lambda)$ is the simulated reflection rate. The single metal layer structure is also simulated, as shown in Fig. 1(b). For the single metal layer structure, the maximum transmittance is achieved (20%) at 407 nm, while the simulated absorption is reduced with wavelength, as shown in Fig. 1(c). Moreover, the simulated reflection is increased with wavelength and reached to 82% at 1 000 nm, as shown in Fig. 1(c). When a dielectric layer is covered above the metal layer, the optical property shows a dramatic change. For the proposed structure, the simulated transmission shows a peak (38%) at 502 nm, as shown in Fig. 1(d). At the same time, the simulated absorption shows a peak at the resonance wavelength 498 nm, as shown in Fig. 1(d). Synchronously, the simulated reflection achieves a valley near to zero (1%) at 498 nm. These results indicate that simulated transmission and absorption are enhanced due to cover a dielectric layer on the metal layer. Multilayer film is a material with high application value. Most of multilayer films are demonstrated to achieve high absorption loss at optical frequencies [24-27]. However, in order to obtain a high absorption rate, such materials often require the deposition of different types of films, resulting in a complicated structure and an increase in manufacturing cost. For example, *Chenying Yang et al* propose and measure an Ag/Si/Cr/TiO_2 multilayer films for angle robust color filtering [28]. *Timothy D. Corrigan et al* design a broadband multilayer films absorber through stacking up to 21 layers of film [29]. *Mehdi Keshavarz Hedayati et al* manufacture an Au/SiO_2/ nanocomposite multilayer films absorber with a broad absorption band from 400 ~ 750 nm [30]. Comparing these reported multilayer film structural materials, the proposed multilayer films in this paper reveals two characteristics: (a) the proposed multilayer films just consists of only two layers of material, and the dielectric layer is a readily available and low cost material. (b) The absorption and transmittance are simultaneously enhanced.

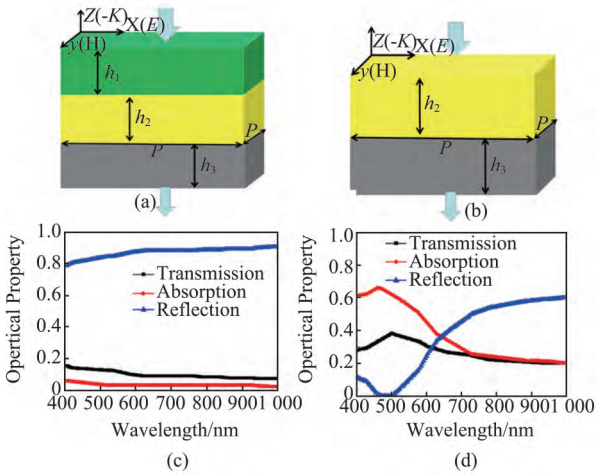

Fig. 1　(a) Three-dimensional image of the proposed compact metal-dielectric double-layered films. (b) Three-dimensional image of the single layered film. (c) Transmission, absorption, and reflection of the single silver layer film. (c) Transmission, absorption, and reflection of the proposed compact metal-dielectric double-layered films. The green part is the $CaCO_3$ layer. The yellow part is the metal layer. The gray part is the glass substrate

图 1　(a) 所提出的金属-电介质双层膜的三维图像. (b) 单层膜的三维图像. (c) 单银层膜的透射,吸收和反射. (c) 所提出的金属-电介质双层膜的透射,吸收和反射. 绿色部分是 $CaCO_3$ 层. 黄色部分是金属层. 灰色部分是玻璃基板

2　Simulation results and discussion

2.1　Physical mechanism

Table 1 Dimensional parameters of the proposed double layer structure

表1 所提出的双层结构的尺寸参数

Parameters	P	h_1	h_2	h_3
Value(nm)	100	8	34	40

To understand the physics behind the transmission and absorption spectrum in Fig. 1(c-d), simulated electric field profile of the proposed structure across all layers is calculated, as shown in Fig. 2. For research convenience, the electric field of the single metal layer structure is also calculated, as shown in Fig. 2(a). It can be found that high value of electric field profile is achieved on the surface of the metal layer. In order to measure the electric field strength, a test point is selected 2 nm below the surface of the metal layer, as shown in Fig. 2. The single metal layer shows an obvious reflection on the metal layer surface at 508nm, which indicates a standing wave is achieved. However, inside the metal layer, the electric field intensity is drastically weakened, which indicates that the transmission or absorption of the single metal layer is low, as shown in Fig. 2(a). For the proposed structure, four calculating wavelengths are selected in simulation (465 nm, 508 nm, 560 nm, and 800 nm), as shown in Fig. 2(b-e). For the calculating wavelength at 465 nm, a similar electric field distribution is found on the surface of the dielectric layer. However, the electric field intensity at the testing point in Fig. 2(b) is obviously higher than that in Fig. 2(a). Moreover, strong electric field distribution is found inside the dielectric and metal layers, which implies that higher absorption and transmission are obtained in dielectric layer and metal layer, respectively. Moreover, the electric field distribution in the dielectric and metal layers is further enhanced at wavelength 508 nm in Fig. 2(c), which results in the absorption and transmission peaks in Fig. 1(d). However, the electric field distribution in dielectric and metal layers is reduced at wavelength 560 nm and 800 nm in Fig. 2(d-e), which leads to the absorption and transmission reduce in Fig. 1(d). These results in Fig. 1(c-d) and Fig. 2(a-e) indicate that the proposed compact metal-dielectric double-layered films can achieve higher transmission than that of the single metal layer structure. In order to analyze the electric field intensity distribution characteristics of both structures, the electric field resonance enhanced factor is adopting in this paper, as following:

$$\sigma = \left|E_{Ag+Si}\right| / \left|E_{Ag}\right| \quad , \quad (2)$$

In the equation (2), the calculated electric field ($|E|$) is tested in simulation at a fixed point which is 2 nanometers below the surface of the metal layer, as shown in Fig. 2(a-e). The electric field resonance enhanced factor spectrum is shown in Fig. 3. It is obviously that the proposed compact metal-dielectric double-layered films can achieve higher electric field distribution. The maximum electric field distribution intensity is 70 times of the single metal layer structure, as shown in Fig. 3. At the same time, a higher transmission is achieved, as shown in Fig. 1.

In order to further reveal the resonance properties of the compact metal-semiconductor double-layered films, an S-parameter extraction method is employed [31-32]. The effective parameters extracted include effective permittivity ε_{eff}, permeability μ_{eff}, refractive index n_{eff}, and impedance z_{eff}, as shown in Fig. 4 It is found that the real part of ε_{eff} is 1.12, and the real part of μ_{eff} is 1.02. Therefore, the effective impedance of z_{eff} the compact metal-semiconductor double-layered films is given as following:

$$z_{eff} = \sqrt{\mu_{eff}} / \sqrt{\varepsilon_{eff}} \quad , \quad (3)$$

The real part of z_{eff} is 0.92 at the transmission peak wavelength 502 nm. This strong electromagnetic resonance behavior leads to a impedance matching phenomenon between the compact metal-semiconductor double-layered films and the free space, which results in the transmission enhancement. Moreover, the imaginary part of z_{eff} is $-0.03i$ at the reflection peak wavelength 498nm, which implies the reflection of the electromagnetic wave energy on the silver layer surface is reduced. At the same time, the effective refractive index n_{eff} is given as following:

$$n_{eff} = \sqrt{\varepsilon_{eff}} \cdot \sqrt{\mu_{eff}} \quad , \quad (4)$$

The real part of n_{eff} is 1.65 and the imaginary part is $+4.27i$ at the absorption peak wavelength 498 nm. The large imaginary part of n_{eff} indicates that the absorption

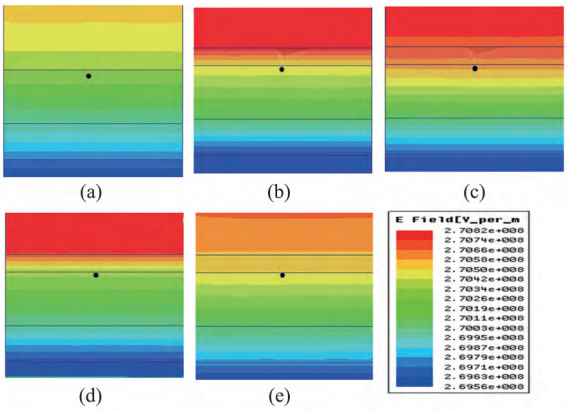

Fig. 2 Simulated electric field distributions at different resonance wavelength. The black point in figures is the electric field strength test point

图2 不同共振波长下的模拟电场分布. 图片中的黑点是电场强度测试点

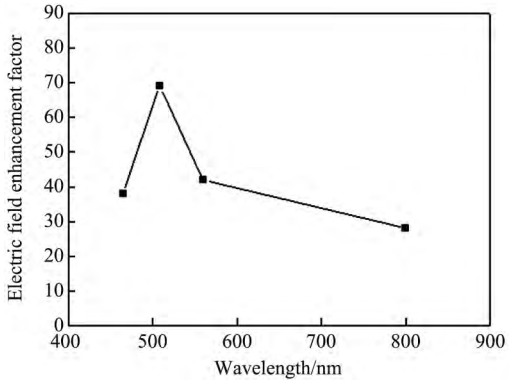

Fig. 3 The electric field resonance enhanced factor at different resonance wavelength

图3 不同共振波长下的电场共振增强因子

loss of electromagnetic wave energy in the $CaCO_3$ layer is enhanced at the same time, as shown in Fig. 2(b-c). These electromagnetic resonance behaviors result in an increase in transmission and absorption, and a decrease in reflection. When electromagnetic waves are incident on the surface of the single silver layer structure, most of the energy is reflected (transmission and absorption are small), so the electric field strength on the surface and inside of the silver layer is at a low level, as shown in Fig. 2(a). When the electromagnetic waves are incident on the surface of the compact metal-semiconductor double-layered films, the transmission and absorption are both enhanced (the reflection is reduced) due to these strong resonance behavior in Fig. 4. Therefore, the electric field strength on the surface and inside of the $CaCO_3$ layer and silver layer is increased, as shown in Fig. 2(b-c). These results in Fig. 2 and Fig. 4 indicate that the electromagnetic properties of the entire multilayer film structure are greatly improved by covering a layer of $CaCO_3$ layer on a single silver layer.

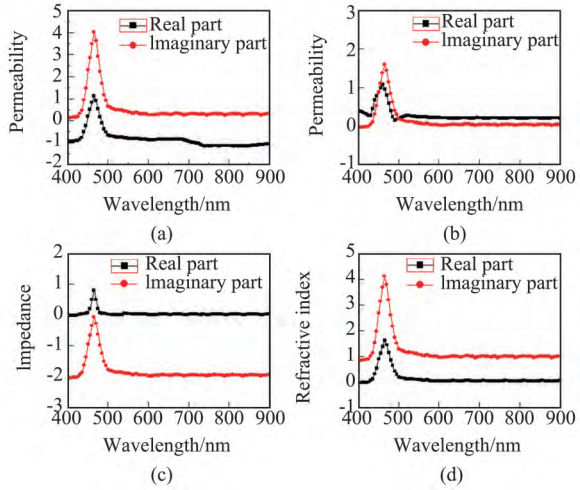

Fig. 4　The extracted effective parameters. (a) The effective permittivity ε_{eff}. (b) The effective permeability μ_{eff}. (c) The effective impedance z_{eff}. (d) The effective refractive index n_{eff}

图 4　提取的有效参数. (a) 有效介电常数 ε_{eff}. (b) 有效磁导率 μ_{eff}. (c) 有效阻抗 z_{eff}. (d) 有效折射率 n_{eff}

2.2　Dielectric layer thickness optimization

To exploit the effect of the thickness h_1 on the transmission enhancement, a set of simulations is carried out, while other structural parameters remain unchanged. Fig. 5 shows the transmission spectrum of the proposed compact metal-dielectric double-layered films with different thickness h_1. When h_1 is increased from 8 nm to 12 nm, transmission peak is enhanced to 43% at 561 nm and the electric field resonance enhanced factor is 2.3. When h_1 = 20 nm, a maximum transmission 51% is achieved at 640 nm. However, when h_1 is larger than 20 nm, the transmission peak is reduced. The transmission peak shows a shifted to longer resonant wavelength with h_1 increasing. For the single metal layer structure, the maximum transmission value is 20% at 407 nm. Resonant transmission enhancement is achieved when a dielectric layer with appropriating thickness is covered on the metal layer. These results indicate that the transmission enhancement can be manipulated by optimizing the dielectric thickness h_1. The transmittance enhancement factor is adopted to reveal the relationship between the dielectric layer thickness and the transmission enhancement, as following:

$$\delta = T_{doublelayers}/T_{singlelayer} \quad , \quad (5)$$

Here, T_{double} is the transmission of the proposed structure, and $T_{single\ layer}$ is the transmission of the single metal layer structure. It can be found that the transmittance enhancement factor is increased with the dielectric layer thickness h_1 increasing, as shown in Fig. 6. However, maximum values of transmittance enhancement factor are not exact consistent with transmission peaks. It is because that the transmission spectrum of the single layer structure shows a steep slope in 540 ~ 630 nm, which leads to the transmittance ratio increase.

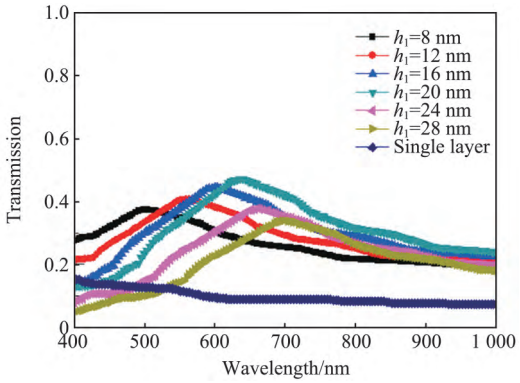

Fig. 5　Simulated transmission spectrum with different dielectric layer thickness

图 5　具有不同介电层厚度的模拟透射光谱

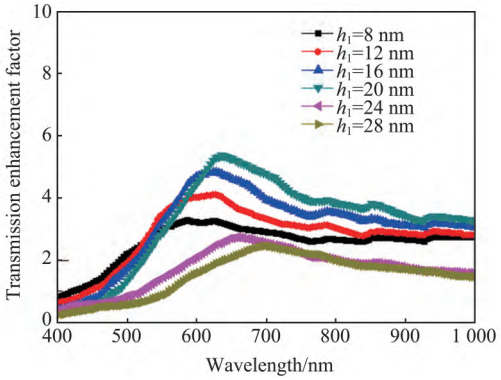

Fig. 6　Transmission enhancement factor spectrum with different dielectric layer thickness

图 6　具有不同介电层厚度的透射增强因子光谱

According to the equation (1), simulated transmission value is directly defined by the simulated absorption and reflection. In order to comprehensively study the optical properties of the proposed compact metal-dielectric double-layered films, simulated absorption and reflection are also calculated in simulation, as shown in Figs 7 and 8. For a 8nm-thick dielectric layer coating on the metal layer, the simulated reflection is reduced obviously, as

shown in Fig. 7. It is found that a simulated reflection valley near to 1% is achieved at 498 nm. When h_1 is increased from 8 nm to 20 nm, the reflection shows a slightly increased. The reflection valley is increased to 12% (thickness is 20 nm). When thickness $h1 > 20$ nm, the reflection valley shows a slightly reduced. Moreover, the reflection valley shows a shifted to longer wavelength with $h1$ increasing, as shown in Fig. 7. At the same time, absorption peaks are obtained with different $h1$, as shown in Fig. 8. The absorption peak shows an increase with $h1$ increasing. The simulated reflection and absorption of the single structure is also provided in Fig. 7 and 8. For the single structure, the reflection shows an increase with wavelength and reaches 82% at 1 000 nm. However, the simulated absorption is reduced with wavelength and reaches 7% at 1 000 nm. In contrast to the presence or absence of a dielectric layer in Figs 7 and 8, it can be found that the simulated transmission is significantly enhanced after covering a dielectric layer on the metal layer. The simulated absorption is also enhanced.

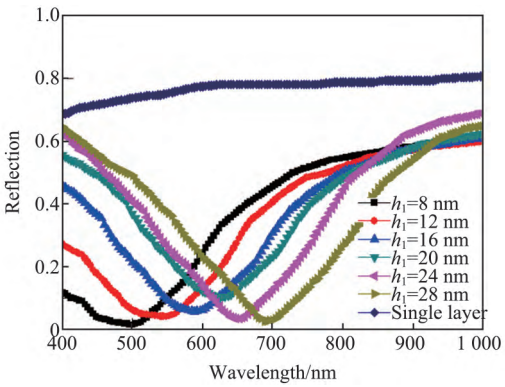

Fig. 7 Simulated reflection spectrum with different dielectric layer thickness

图7 具有不同介电层厚度的模拟反射光谱

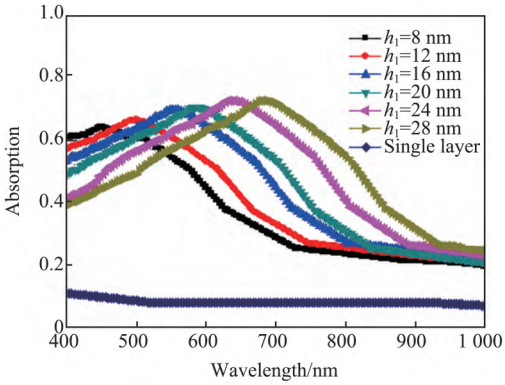

Fig. 8 Simulated absorption spectrum with different dielectric layer thickness

图8 具有不同介电层厚度的模拟吸收光谱

2.3 Transmission enhancement with incident angle

Fig. 9 shows the transmission spectrum with different incident angle. The incident angle is increased from 0° to 45° in simulation. It can be found that the transmission peak shows a slight reduction when the incident angle is increased to 30°. When the incident angle is increased to 45°, the transmission peak is reduced to 32%, only decreased by 6%. These results indicate that the proposed compact metal-dielectric double-layered films achieve stability of enhanced optical transmission to incident angle.

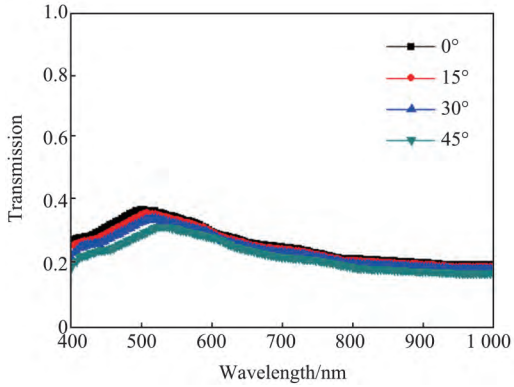

Fig. 9 Simulated transmission spectrum with different incident angle

图9 具有不同入射角的模拟透射光谱

3 conclusions

In this paper, we proposed a compact metal-dielectric double-layered film with a continuous dielectric film covering on a continuous metallic layer. It is found that the transmission can be enhanced obviously comparing the single metal layer structure. Moreover, the absorption is also enhanced while the reflection is reduced simultaneously. High stability of transmittance enhancement is shown when the incident angle reaches 45°. Since the proposed compact metal-dielectric double-layered film is non-hollowing structure, this structure can be large-scale and low cost manufactured in many potential fields.

References

[1] Zhu X F, Li K, Zhang P, *et al*. Implementation of dispersion-free slow acoustic wave propagation and phase engineering with helical-structured metamaterials [J]. *Nature Communications*, 2016, **7**: 11731-11738.

[2] Nguyen D M, Lee D, Rho J. Control of light absorbance using plasmonic grating based perfect absorber at visible and nearinfrared wavelengths [J]. *Scientific Reports*, 2017, **7**: 2611-2618.

[3] Lai C H, Wang G A, Ling T K, *et al*. Near infrared surface-enhanced Raman scattering based on starshaped gold/silver nanoparticles and hyperbolic metamaterial, *Scientific Reports*, 2017, **7**: 5446-5453.

[4] Galutin Y, Falek E, Karabchevsky A. Invisibility Cloaking Scheme by Evanescent Fields Distortion on Composite Plasmonic Waveguides with Si Nano-Spacer, *Scientific Reports*, 2017, **7**: 12076-12083.

[5] Liu Z G, Lu W B, Yang W. Enhanced Bandwidth of High Directive Emission Fabry-Perot Resonator Antenna with Tapered Near-Zero Effective Index Using Metasurface, *Scientific Reports*, 2017, **7**: 11455-11464.

[6] Xomalis A, Demirtzioglou I, Plum E, *et al*. Fibre-optic metadevice for all-optical signal modulation based on coherent absorption [J]. *Nature Communications*, 2018, **9**: 182-189.

[7] Rodrigues S P, Lan S F, Kang L, *et al*, Intensity-dependent modulation of optically active signals in a chiral metamaterial [J]. *Nature Communications*, 2017, **8**: 14602-14469.

(下转第330页)

[4] Y. Yan K M J, M. M. Al-Jassim. Atomic Structure of Twin Boundaries in CdTe [J]. *National Center for Photovoltaics and Solar Program Review Meeting*, 2003.
[5] Zeng D M, Jie W Q, Wang T, *et al*. Transmission electron microscopy observations of twin boundaries and sub-boundary networks in bulk CdZnTe crystals [J]. *Journal of Crystal Growth*, 2009, **311**(19): 4414-4417.
[6] Zhu J Q, Chu J H, Zhang X P, *et al*. Study of zinc inclusions/precipitates in CdZnTe crystals [J]. *Journal of Crystal Growth*, 1997, **171**(3-4): 357-360.
[7] Bolotnikov A E, Abdul-Jabbar N M, Babalola O S, *et al*. Effects of Te Inclusions on the Performance of CdZnTe Radiation Detectors [J]. *Ieee Transactions on Nuclear Science*, 2008, **55**(5): 2757-2764.
[8] Sheng F F, Zhou C H, Sun S W, *et al*. Influences of Te-Rich and Cd-Rich Precipitates of CdZnTe Substrates on the Surface Defects of HgCdTe Liquid-Phase Epitaxy Materials [J]. *Journal of Electronic Materials*, 2014, **43**(5): 1397-1402.
[9] Clajus M, Tumer T O, Visser G I, *et al*. Scanned x-ray images from a linear CdZnTe pad array with monolithic readout electronics [J]. *Hard X-Ray Gamma-Ray and Neutron Detector Physics Ii*, 2000, **4141**: 274-280.
[10] Jeoung Y, Lee T, Kim H, *et al*. New method of the determination of HgCdTe/CdZnTe composition by infrared transmission [J]. *Japanese Journal of Applied Physics Part 1-Regular Papers Short Notes & Review Papers*, 1996, **35**(1a): 134-139.
[11] Huang G S, Yang J R, Chen X Q, *et al*. Study of interdiffusion in HgCdTe/CdZnTe structures by infrared transmission spectroscopy [J]. *Fourth International Conference on Thin Film Physics and Applications*, 2000, **4086**: 270-273.
[12] Hou Q R, Chen Y B, Chen H, *et al*. Characterization of CdZnTe crystals by resistivity measurements and chemical etching [J]. *Modern Physics Letters B*, 2002, **16**(17): 615-619.
[13] Benson J D, Bubulac L O, Jaime-Vasquez M, *et al*. Analysis of Etched CdZnTe Substrates [J]. *Journal of Electronic Materials*, 2016, **45**(9): 4502-4510.
[14] Chen L, Zhang S Y. Photothermal Detection for Light-Scattering Material by Laser Interferometry [J]. *Applied Physics Letters*, 1987, **50**(19): 1340-1342.
[15] Penchev S, Pencheva V, Nedkov I, *et al*. Laser Photothermal Analysis of Magnetoelectric Materials [J]. *7th International Conference of the Balkan Physical Union Vols* 1 *and* 2, 2009, **1203**: 273-276.
[16] Dong J T, Chen J, Sun S W, *et al*. Evaluation of surface and bulk qualities of semiconductor materials by a laser-induced photothermal technique [J]. *Third International Symposium on Laser Interaction with Matter*, 2015, 9543.
[17] CAPPER P, J G. Mercury Cadmium Telluride: Growth, Properties and Applications [J]. *Wiley Series in Materials for Electronic and Optoelectronic Applications*, 2011.
[18] Jin zhonghui. university Fundamental Physics; [M](金仲辉. 大学基础物理学), 2000. 311.

(上接第324页)

[8] Barnes W L, Murray W A, Dintinger J, *et al*, Surface Plasmon Polaritons and Their Role in the Enhanced Transmission of Light through Periodic Arrays of Subwavelength Holes in a Metal Film [J]. *Ph Ysica L R Ev I Ew L Et T Ers*, 2004, **9**: 107401-107404.
[9] Zhang X Q, Gu J Q, Cao W, *et al*, Bilayer-fish-scale ultrabroad terahertz bandpass filter [J]. *Optics Letters*, 2012, **37**: 906-908.
[10] Han N R, Chen Z C, Lim C S, *et al*. Broadband multi-layer terahertz metamaterials fabrication and characterization on flexible substrates [J]. *Optics Express*, 2011, **19**: 6990-6998.
[11] Lan F, Yang Z Q, Qi L M, *et al*, Terahertz dual-resonance bandpass filter using bilayer reformativecomplementary metamaterial structures [J]. *Optics Letters*, 2014, **39**: 1709-1711.
[12] Krishnan A, Thio T, JKim T, *et al*, Evanescently coupled resonance in surface plasmon enhanced transmission [J]. *Optics Communications*, 2001, **200**: 1-7.
[13] Liang L J, Jin B B, Wu J B, *et al*, A flexible wideband bandpass terahertz filter using multi-layer metamaterials [J]. *Appl. Phys. B*, 2013, **113**: 285-290.
[14] WANG L, GENG Z X, HE X J, *et al*, Realization of band-pass and low-pass filters on a single chip in terahertz regime [J]. *Optoelectronics Letters*, 2015, **11**: 33-35.
[15] Zhong M, Experimental and numerical study of a broad pass-band low-loss optical metamaterials filter [J]. *Optical Materials*, 2015, **47**: 62-66.
[16] Kats M A, Sharma D, Lin J, *et al*, Ultra-thin perfect absorber employing a tunable phase change material [J], *Applied Physics Letters*, 2012, **101**: 221101-221106.
[17] Kats M A, Blanchard R, Ramanathan S, *et al*, Thin-film interference in lossy, ultra-thin layers [J]. *Opt. Photonics News*, 2014, **25**: 40-47.
[18] Dotan H, Kfir O, Sharlin E, Oshri Blank *et al*, Resonant light trapping in ultrathin films for water splitting [J]. *Nat. Mater*. 2013, **12**: 158-164.
[19] Corrigan T D, Park D H, Dennis Drew H, *et al*, Broadband and mid-infrared absorber based on dielectric-thin metal film multilayers [J], *APPLIED OPTICS* 2012, **51**: 1109-1114.
[20] Yang C Y, W Shen W D, Zhang Y G, *et al*, Compact Multilayer Film Structure for Angle Insensitive Color Filtering [J]. *Scientific Reports*, 2015, **5**: 9285-95.
[21] Ji D X, Song H M, Zeng X, *et al*, Broadband absorption engineering of hyperbolic metafilm patterns [J]. *Scientific Reports*, 20104, **4**: 4498-4506.
[22] Dong Z G, Zhu S N, Liu H, Numerical simulations of negative-index refraction in wedge-shaped metamaterials [J]. *Phys Rev E*, 2005, **72**: 016607-016610.
[23] Zhang S, Fan W J, Paniou N C, *et al*, Experimental demonstration of near-infrared negative index metamaterials [J]. *Phys. Rev. Lett.* 95(2005): 137404-137407.
[24] Kats M. A., Blanchard R., Ramanathan S. *et al*, ultra-thin layers. *Opt. Photonics News*, 2014, **25**: 40-47.
[25] Cleary J. W, Soref R,. Hendrickson J R. Long-wave infrared tunable thin film perfect absorber utilizing highly doped silicon-onsapphire [J]. *Opt. Express* , 2013, **21**: 19363-19374.
[26] Ding F, Cui Y X, Ge X C, Ultra-broadband microwave metamaterial absorber [J]. *Applied Physics Letters*, 2012, **100**: 103506-103509.
[27] Yi J J, Piau G P, André de Lustrac, *et al*, Electromagnetic field tapering using all-dielectric gradient index materials [J]. *Scientific Reports*, 2016, **6**: 30661-30667.
[28] Yang C Y, Shen W D, Zhang Y G, *et al*, Compact Multilayer Film Structure for Angle Insensitive Color Filtering [J]. *Scientific Reports*, 2015, **5**: 9285-9289.
[29] Corrigan T D, Park D H, Dennis H, *et al*, Broadband and mid-infrared absorber based on dielectric-thin metal film multilayers [J]. *Applied Optics*, 2012, **51**: 1109-1114.
[30] Hedayati M K , Javaherirahim M, Mozooni B, *et al*, Design of a Perfect Black Absorber at Visible Frequencies Using Plasmonic Metamaterials [J]. *Adv. Mater*. 2011, **23**: 5410-5414.
[31] Mary A, Rodrigo S G, Garcia-Vidal F G, *et al*, Theory of negative-refractive-index response of double-fishnet structures [J]. *Phys. Rev. Lett*. 2008, **101**: 103902-103905.
[32] Smith D R, Vier D C, Koschny T, *et al*, Electromagnetic parameter retrieval from inhomogeneous metamaterials [J]. *Phys. Rev. E*, 2005, **71**: 036617-036627.